crystals

MDPI

Article

Crystal Structure and Behavior of the Cocrystal Salt (±)Ibuprofen$_2$HK

Elisa Collet Salvet [1,2], Morgane Sanselme [1], Yohann Cartigny [1], Céline Rougeot [2], Raphael Teixeira [2] and Gérard Coquerel [1,*]

[1] SMS, UR 3233, University Rouen Normandie, 76000 Rouen, France; elisa.collet@univ-rouen.fr (E.C.S.); morgane.sanselme@univ-rouen.fr (M.S.); yohann.cartigny@univ-rouen.fr (Y.C.)
[2] Analytical Characterization Laboratories, Sanofi, 371 rue du Pr. Joseph Blayac, 34184 Montpellier, France; celine.rougeot@sanofi.com (C.R.); raphael.teixeira@sanofi.com (R.T.)
* Correspondence: gerard.coquerel@univ-rouen.fr

Abstract

Salt formation is a key strategy to optimize the physicochemical properties of active pharmaceutical ingredients. The synthesis and characterization of a 2:1 cocrystal salt of racemic ibuprofen with potassium, (±)Ibu$_2$HK, are reported, and the salt is identified as a Speakman salt. Single-crystal X-ray diffraction reveals an asymmetric unit containing three independent ibuprofen molecules and 1 + 0.5 potassium cations occupying two distinct coordination environments, with two short carboxyl–carboxylate O···O contacts (2.437 and 2.447 Å), each bridged by a shared hydrogen atom. The behaviors of the cocrystal salt (±)Ibu$_2$HK and the salt (±)IbuK are also compared. (±)Ibu$_2$HK shows negligible moisture uptake (<0.5%) across the 0–90% RH range, in contrast to the deliquescent behavior of (±)IbuK. Upon heating, (±)Ibu$_2$HK melts at 121 °C and dissociates into recrystallized (±)IbuK and evaporated (±)IbuH, with a mass loss of 48.4 wt% measured by TGA-DSC, consistent with the theoretical value of 45.8 wt%. In water, (±)Ibu$_2$HK fully dissociates as well, firstly releasing the ionic species (±)Ibu$^-$ and K$^+$ into solution while (±)IbuH precipitates. Thus, the pH of the resulting suspension is always higher than the pKa of the acid.

Keywords: Rac-ibuprofen; cocrystal salt; Speakman salt; deliquescence; full dissociation in water

1. Introduction

The physicochemical properties of an active pharmaceutical ingredient (API), including aqueous solubility, dissolution rate, bioavailability, hygroscopicity, stability and processability, depend on its solid form [1,2]. Several strategies are used to improve these properties, the most common being the screening of new solid forms, i.e., polymorphs, salts and/or cocrystals [1–5]. Salt formation remains the most widely used strategy for ionizable APIs, with approximately more than 50% of APIs commercialized as salts [3,6].

In some cases, three or more components can crystallize within a shared crystal lattice, leading to hybrid solids such as cocrystal salts, solvated salts or solvated cocrystals [7]. Of particular interest in this work is the cocrystal salt, a multicomponent solid in which one molecule of the protonated acid (HA) and one molecule of the deprotonated acid (A$^-$) coexist with a single cation (M$^+$) in a 2:1 ratio (HA·A$^-$·M$^+$).

Several hybrids of the HA·A$^-$·M$^+$ type have been reported in the literature. Divalproex sodium (Depakote™), a 1:1 cocrystal salt of valproic acid and sodium valproate approved for the treatment of epilepsy, provides a non-hygroscopic solid compared with the pure

Check for updates

Academic Editor: Borislav Angelov

Received: 31 August 2026
Revised: 22 September 2026
Accepted: 23 September 2026
Published: 26 September 2026

Copyright: © 2026 by the authors. Licensee MDPI, Basel, Switzerland. This article is an open access article distributed under the terms and conditions of the Creative Commons Attribution (CC BY) license.

sodium salt [8]. Along with the 2:1 cocrystal of benzoic acid with sodium benzoate [9] and the sodium glycolate–glycolic acid compound [10], these are three well-characterized examples of this type.

When characterizing cocrystal salts of the $HA{\cdot}A^{-}{\cdot}M^{+}$ type, one of the challenges lies in the localization of the bridging proton in between the two carboxyl groups. On this subject, the work of Speakman has been widely used to comprehend the position of the bridging hydrogen atom. It focuses on the geometry and length of O–H···O hydrogen bonds. A first description in 1949 [11] was followed by a more detailed review in 1972 on the geometry of short hydrogen bonds in salts of monobasic carboxylic acids [12]. The two carboxyl groups are connected by a short O–H···O hydrogen bond with an O···O distance typically between 2.40 and 2.55 Å, significantly shorter than the value of approximately 2.65 Å reported in the literature for O–H···O hydrogen bonds between carboxylic moieties [11,12]. Two structural types are described according to the symmetry of the bridging proton. In type A, the two oxygens are related by a symmetry element (most often an inversion center), and the proton is constrained to a single position, equidistant from both oxygen atoms and located at the inversion center. In type B, the two oxygen atoms belong to two distinct molecules, and the proton is non-equidistant to the two oxygen atoms.

Ibuprofen (2-(4-isobutylphenyl)propanoic acid) is a non-steroidal anti-inflammatory drug of the α-arylpropionic acid family, used as an analgesic, antipyretic and anti-inflammatory agent [13]. It is marketed as a racemic mixture, although only the (*S*)-enantiomer is active; in vivo, R-ibuprofen can undergo a chiral inversion [14]. The protonated acid form, (±)IbuH, exhibits a low intrinsic aqueous solubility (0.026 $g{\cdot}L^{-1}$ at 25 °C) [15] and a pK_a of 4.45 [16], which has motivated the development of new solid forms to improve its dissolution profile and bioavailability [6,17]. Both organic and inorganic counterions have been considered for this purpose. Among the organic ones, the L-lysine and L-arginine salts of ibuprofen are commercially available and were developed to increase the dissolution rate of the API [18]. Ibuprofen has also been shown to coordinate alkali metal centers in ternary complexes with 1,10-phenanthroline (CCDC: 2015739) [19]. One example of an inorganic salt developed for this purpose is the sodium salt of (±)Ibuprofen, (±)IbuNa, at ambient humidity, characterized by a strong water uptake leading to a transition into (±)IbuNa.$2H_2O$ [20,21]. Among the alkali metal salts of ibuprofen, the sodium salt (±)IbuNa is by far the most studied. By contrast, the potassium analogue (±)IbuK is not as described in the literature. The available descriptions report it as highly hygroscopic and deliquescent under ambient relative humidity, with no hydrated form identified to date [22]. A 2:1 cocrystal salt of ibuprofen, (±)Ibu_2HK, was disclosed in a 2002 patent by Xu, Erkoboni and Lebo [22] as an alternative crystalline form of potassium ibuprofen with reduced hygroscopicity, but the patent was abandoned in 2007, and neither a structural characterization nor any further study has been published since.

In the present work, we report the single-crystal X-ray structure of (±)Ibu_2HK and characterize it as a hybrid cocrystal salt featuring two short carboxyl–carboxylate hydrogen bonds. Speakman's criteria were applied to determine the location of the bridging hydrogen atom of (±)Ibu_2HK. By comparison, the crystal structure of the equimolar salt (±)IbuK has not been solved to date. Dynamic vapor sorption measurements, aqueous dissolution experiments and thermal analysis are presented as a comparative physicochemical characterization of (±)Ibu_2HK and (±)IbuK.

2. Materials and Methods

(±)Ibuprofen ((±)IbuH) was supplied by Pharmadev, Geneva, Switzerland and KOH was supplied by CARLO ERBA Reagents SAS, Val-de-Reuil, France as pellets; both were used without further purification.

(±)IbuprofenK ((±)IbuK) was synthesized following the procedure previously reported by Xu et al. [22]. An equimolar amount of (±)IbuH (2.399 g) and KOH (0.2812 g) was dissolved in deionized water at 70 °C. The homogeneous solution was transferred to a crystallizer and heated on a hot plate at 75 °C until complete evaporation of the solvent. The resulting layer of white crystals was ground, weighed and resulted in an 86% yield after overnight storage in a 0% desiccator.

The hemi-salt (±)Ibuprofen$_2$H.K ((±)Ibu$_2$HK) was prepared by reacting (±)IbuH (2.0632 g) and KOH (0.2812 g) in a 2:1 molar ratio. Two crystallization routes were used, both leading to a white powder exhibiting the same X-ray powder pattern: (i) dissolution in absolute ethanol at room temperature followed by crystallization at −30 °C overnight, or (ii) dissolution in deionized water at 70 °C followed by evaporation of the solution on a hot plate at 75 °C. The latter resulted in a yield of 92%. The powder thus obtained was used to grow single crystals by evaporation of a saturated solution of (±)Ibu$_2$HK in acetone at room temperature using the sitting-droplet method described in Figure 1 [23]. (±)IbuK and (±)Ibu$_2$HK were stored at 20 °C in a desiccator at 0% RH (P_2O_5) to prevent atmospheric moisture uptake.

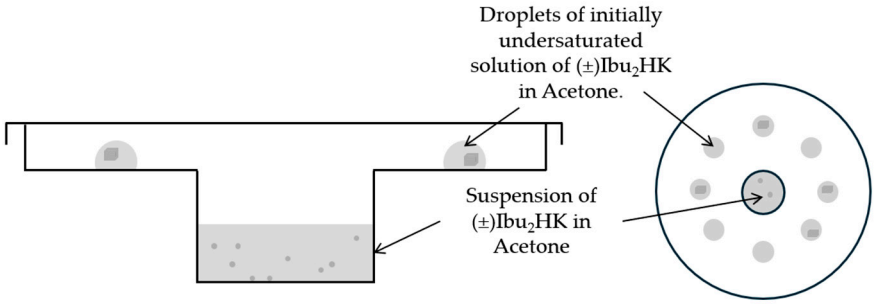


Figure 1. Schematic representation of the custom-made "crystallization mushroom" developed by the crystallization Factoria of IACT used to obtain single crystals of (±)Ibu$_2$HK in acetone at 25 °C. A lower compartment contained a suspension of (±)Ibu$_2$HK and the top layer held a filtered, seeded saturated solution, sealed with a lid and vacuum grease to maintain a closed environment.

2.1. Optical Microscopy, HSM and SEM

Optical microscopic photos were taken with a Eclipse LV100 optical microscope from Nikon corporation, Tokyo, Japan, equipped with a digital sight camera with a pair of cross polarizers. Hot-stage microscopy (HSM) was performed using a THMS 600 hot-stage chamber from Linkam Scientific Instruments Ltd., Redhill, UK.

Scanning electron microscopy (SEM) was used to observe the surfaces of the single crystals of (±)Ibu$_2$HK. Images were collected on a benchtop SEM JCM-5000 NeoScope instrument from JEOL Ltd., Akishima, Tokyo, Japan (in high-vacuum mode: secondary electron imaging) at an accelerated voltage fixed at 10 kV. This device allowed magnifications from ×22 up to ×20,000. The samples were directly fixed on pin stubs using conductive adhesives and then coated with gold (NeoCoater MP-19020NCTR from JEOL Ltd., Akishima, Tokyo, Japan) for 15 min to reduce the charge accumulations during the observation.

2.2. Differential Scanning Calorimetry (DSC)

DSC measurements were performed on a DSC 214 Polyma apparatus from NETZSCH-Gerätbau GMBH, Selb, Germany equipped with an intracooler and purged with nitrogen.

Samples were weighed (5–10 mg) into 25-µL aluminum pans. Data were processed using Netzsch Proteus Analysis software Version 7.1.

2.3. X-Ray Powder Diffraction

2.3.1. Amb RH XRD

X-ray powder diffraction (XRPD) at ambient temperature and humidity was carried out on a D8 Discover from Bruker AXS GMBH, Karlsruhe, Germany using Cu Kα radiation (1.54 Å) and a Ni filter. The samples were scanned over the 3 to 30° (2θ) range with a step of 0.04° and 0.5 s per step.

2.3.2. Dry-Air X-Ray Diffraction

XRPD was carried out under a dry atmosphere (continuous dry N2 flow, to prevent structural changes due to moisture uptake) on a D8 Discover from Bruker Bruker AXS GMBH, Karlsruhe, Germany using Cu Kα radiation (1.54 Å) and a Ni filter. Solid samples were subjected to ten consecutive cycles, each consisting of a 30 min drying step followed by 30 min of acquisition. The range was 2–40° (2θ) with a step size of 0.01° and 0.6 s per step.

2.3.3. Single-Crystal X-Ray Diffraction

The crystal structures were determined from single-crystal diffraction on a D8-VENTURE diffractometer from Bruker AXS GMBH, Karlsruhe, Germany equipped with a PHOTON III C7 detector and dual microfocus sources (IµS 3.0 copper and IµS DIAMOND II Molybdenum). The cell parameters and the orientation matrix of the crystal were preliminarily determined using APEX 4 Software Version 2022.10-1 [24]. Data integration and global cell refinement were performed with SAINT Software Version 8.40B [25]. Intensities were corrected for Lorentz, polarization, decay and absorption effects (SADABS Software Version 8.40B [25]) and reduced to F_O^2. The program package WinGX Version 2026.1 [26] was used for space-group determination, structure solution and refinement.

The standard space group was determined from systematic extinctions and relative F_O^2 of equivalent reflections. The structure was solved by direct methods [27]. Anisotropic displacement parameters were refined for all non-hydrogen atoms. All hydrogen atoms related to carbon atoms were placed from subsequent difference Fourier syntheses and placed with geometrical constraints (SHELXL [27]). Hydrogen atoms related to the acidic groups were located by means of geometrical considerations. The bond lengths observed between carbon and oxygen atoms of the different acidic moieties were the relevant factors to indicate the presence or not of the hydrogen atoms.

2.4. Infrared Measurement

Infrared spectrum measurements were performed on an ATR-FTIR spectrometer (Alpha FT-IR spectrometer from Bruker Optik GMBH, Ettlingen, Germany). All samples were slightly ground before being deposited on the ATR. For each spectrum, a total of 128 scans were recorded at room temperature between 4000 and 400 cm^{-1} with a resolution of 2 cm^{-1}.

2.5. Dynamic Vapor Sorption

Moisture sorption and desorption isotherms of the anhydrous crystalline solid were recorded at 25 °C on a DVS Advantage Automated water sorption analyzer from Surface Measurement Systems Ltd., London, UK. Mass variations of the sample (4 mg) were recorded while relative humidity (RH) was successively increased from 0% to 90% RH by successive steps of 10% RH. The automated analyzer was allowed to proceed to the next step as soon as the mass variation of the sample was less than 5.10^{-4}%.min^{-1}. For each

solid, one sorption and desorption cycle was recorded ((±)Ibu_2HK's cycles took 4 days and (±)IbuK's 13 days).

2.6. TGA-DSC

TGA-DSC analyses were carried out with a STA 409 PC instrument from NETZSCH-Gerätebau GMBH, Selb, Germany. Signals were plotted against time to present the evolution of the weight loss during a 2 h isothermal step at 250 °C. Around 4.6 mg of (±)Ibu_2HK was analyzed in a pierced, sealed aluminum crucible and heated at a rate of 2 °C·min^{-1} from 20 °C to 250 °C, followed by a 120 min isothermal old at 250 °C. Helium was used as a purge gas. Proteus® Software Version 7.1 NETZSCH-Gerätbau GMBH, Selb, Germany was used for data treatment.

2.7. Behavior in Water

The behavior of (±)Ibu_2HK powder was investigated in milli-Q water at 25 °C. Approximately 4 g of (±)Ibu_2HK was suspended in 100 mL of water in a thermostated jacket fixed at 25 °C with continuous magnetic stirring. At different times, from 1 min up to 72 h, the pH was measured with FiveEasy pH meter from Mettler-Toledo AG, Greifensee, Switzerland, the solid in suspension was sampled and filtered for XRPD analyses, and the saturated solution was filtered through a 0.2 µm PVDF syringe filter from VWR International, Radnor, PA, USA. Then, the latter was diluted in milliQ water to be analyzed by High-Performance Liquid Chromatography (HPLC) to quantify the total amount of dissolved ibuprofen. A Hypersil GOLD™ column (150 mm × 4.6 mm, Thermo Fisher Scientific, Waltham, MA, USA) was used, with MeOH/H_2O + 0.1% formic acid (80:20, *v*/*v*) as the mobile phase. Each sample was analyzed in triplicate, and mean values are reported. In addition, various masses of (±)Ibu_2HK were added to 1 mL of milliQ water and stirred for 72 h at 25 °C in a PHMT PSC24 thermoshaker from Grant-bio, Grant Instrument Ltd., Shepreth, UK. The masses ranged from 1 to 70 mg of powder (±)Ibu_2HK. The resulting solution was analyzed following the same protocol described above to obtain the pH and the concentrations of (±)Ibu^- and (±)IbuH after 72 h.

3. Results

3.1. Structural Determination and Characterization of (±)Ibu_2HK

3.1.1. Structural Determination of (±)Ibu_2HK

The structure of (±)Ibu_2HK was determined by single-crystal X-ray diffraction (SCXRD) at 170 K. Crystals exhibit a thin-plate morphology, which is actually a stacking of lamellae (Figure 2); this limits the quality of the data. Nevertheless, the final refinement cycle led to acceptable R factors (see Table 1). The analysis of the data does not indicate the presence of twinning; no obvious multiple domains were detected. Nevertheless, inappropriate alignment of the laminated crystal leads to poor-quality data due to high mosaicity. In contrast, the structure of (±)IbuK could not be determined, as its high hygroscopicity prevented the growth of single crystals suitable for X-ray diffraction.

Table 1. Crystallographic data and structure refinement parameters for (±)Ibu_2HK determined from SCXRD.

Compound Reference	CCDC 2579228
Chemical formula	K1.5[C13H17·5O2]3
Crystal system	Monoclinic
a/Å	43.550(3)
b/Å	6.7987(5)
c/Å	26.482(2)

Table 1. *Cont.*

Compound Reference	CCDC 2579228
α/°	90
β/°	104.195(2)
γ/°	90
Unit cell volume/Å3	7601.5(9)
Calculated density	1.181
Temperature/K	170(2)
Space group	C2/c
No. of formula units per unit cell, Z, Z′	8, 1 *
Absorption coefficient, μ/mm^{-1}	0.237
No. of reflections measured	185468
No. of independent reflections	8756
Rint	0.121
Index range	1.929 to 27.562
Completeness to theta 25.242	99.9
Data/restraints/parameters	8756/0/431
Final R1 and wR(F2) values (I > 2σ(I))	R1 = 0.0727, wR2 = 0.1532
Final R1 and wR(F2) values (all data)	R1 = 0.0878, wR2 = 0.1616
Goodness of fit on F2	1.099
Largest diff. peak and hole (e·Å^{-3})	0.896 and −0.392

*: Z′ is composed of 3 independent ibuprofen molecules and 1.5 potassium cations (see chemical formula).

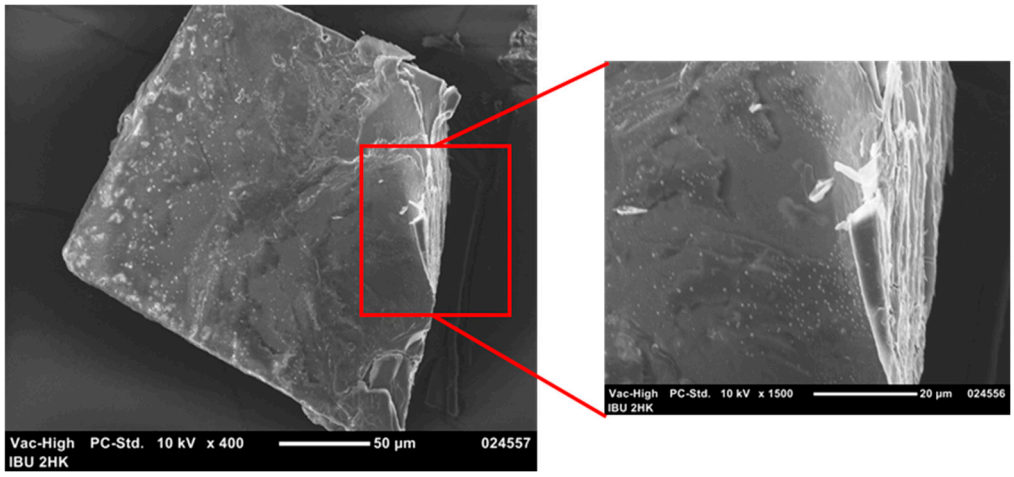


Figure 2. SEM capture and zoom of a single crystal of (±)Ibu$_2$HK. The crystal exhibits a laminated structure.

3.1.2. Structural Description of (±)Ibu$_2$HK

The asymmetric unit is composed of three molecules of ibuprofen (Mol-O, Mol-A and Mol-B hereafter), and 1.5 potassium cations (Figure 3). Ibuprofen molecules and potassium cation K2 are on Wyckoff position 8f, whereas potassium cation K1 is on Wyckoff position 4e. Therefore, there are 1.5 potassium cations for three ibuprofen molecules in the asymmetric unit. For the three ibuprofen molecules, the equivalent isotropic displacement parameters show significantly higher values for the isobutyl groups (Figures S1 and S2), which is an additional contribution to the elevated R factor.

Interactions between consecutive molecules along the *a* axis lead to dimers of Mol-A/Mol-A and Mol-B/Mol-O (Figure 4). Considering the C-O bond lengths (Table 2), none of the carboxyl groups is clearly deprotonated. This could be explained by the Speakman effect, where one hydrogen atom is shared between two adjacent carboxyl groups.

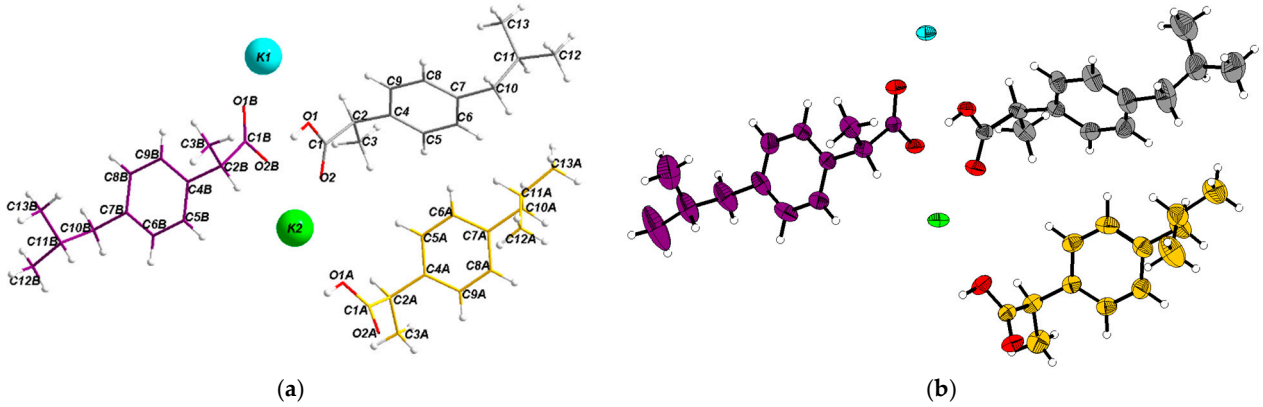


Figure 3. (**a**) Asymmetric unit with atom labels. Ibuprofen molecules are displayed in three different colors (Mol-O in grey, Mol-A in yellow, and Mol-B in purple). Potassium cation K1 (4e Wyckoff site) is displayed in blue, and potassium cation K2 (8f Wyckoff site) is displayed in green. (**b**) Asymmetric unit in thermal ellipsoid representation. Ibuprofen molecules are displayed in three different colors (Mol-O in grey, Mol-A in yellow, and Mol-B in purple). Potassium cation K1 (4e Wyckoff site) is displayed in blue, and potassium cation K2 (8f Wyckoff site) is displayed in green.

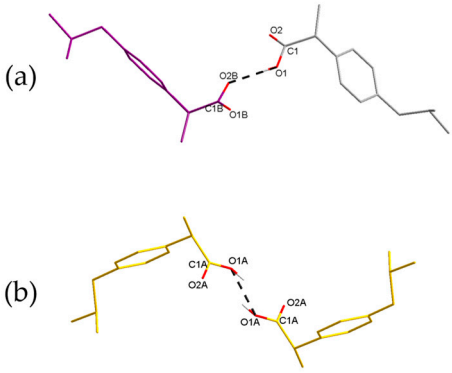


Figure 4. Adjacent interactions involving the Speakman effect of type B for Mol-B and Mol-O and of type A for 2 Mol-A. (**a**) Dimers of Mol-B and mol-O interacting through their acidic function. d(O2B-O1)~2.45Å—dashed black line. (**b**) Dimers of two mol-A interacting through their acidic functions (d(O1A-O1A)~2.46Å—dashed black line.

Table 2. Bond lengths of the carboxyl groups of the three ibuprofen molecules (Å).

	O1 *	**O2 ***
C1	1.296(3)	1.233(3)
C1A	1.290(3)	1.222(3)
C1B	1.232(3)	1.283(3)

*: Oxygen atoms from Mol-O, Mol-A or Mol-B.

According to the Speakman effect, dimers of Mol-A are of type A: the interaction involves two molecules related by an inversion center, and dimers of Mol-B/ Mol-O are of type B; the molecules involved are not related by a symmetry element. Thus, since half of the three ibuprofen molecules are shared, the resulting overall negative charge is consistent with the 1.5 potassium cations present in the asymmetric unit. The localization of this hydrogen atom is described in detail in Supplementary Materials (Figures S3 and S4).

The cohesion of the structure is ensured by the potassium cations that are intercalated between dimers along the *b* and *c* axes (Figure S5). It is worth noting that the coordination polyhedron of the potassium cations K2 is a square-based pyramid (Figure 5). The *bc* layers are stacked along an axis by means of weak interactions (Figure 6).

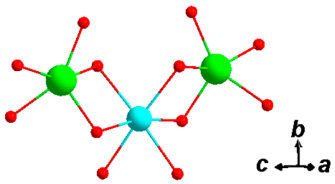


Figure 5. Coordination polyhedra of potassium cations K1 (blue) and K2 (green) are a distorted octahedron and square-based pyramid, respectively.

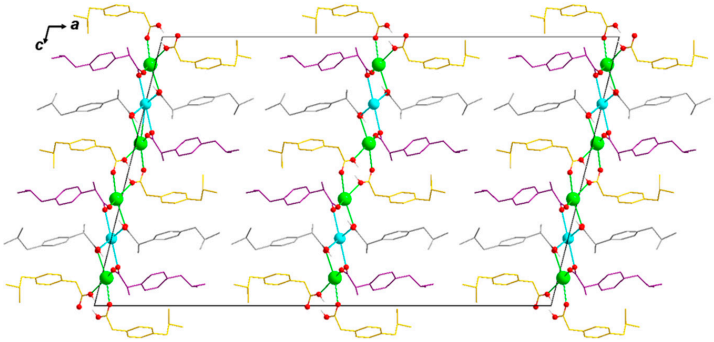


Figure 6. Projection along the b axis of the crystal packing. Layers are stacked along an axis, and they interact through weak interactions involving their isobutyl moieties.

3.2. XRPD Patterns Comparison Between (±)IbuK and (±)Ibu$_2$HK

A comparison between calculated and experimental powder patterns of (±)Ibu$_2$HK is shown in Figure 7. Both match well, and both differ from the pattern obtained for (±)IbuK.

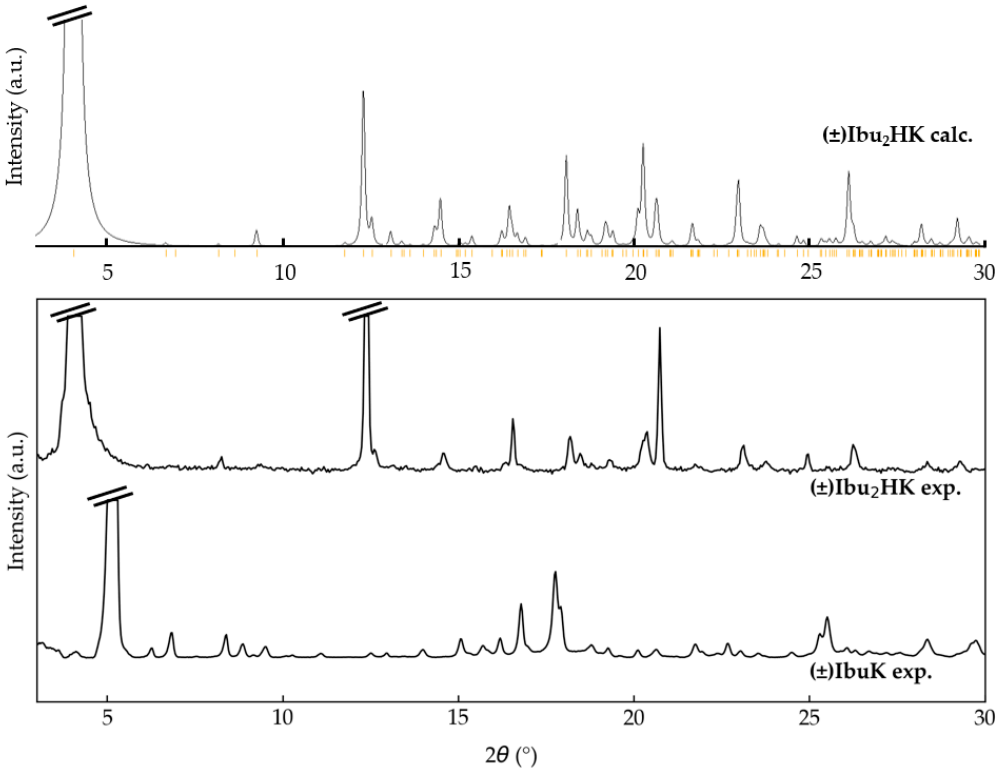


Figure 7. Calculated XRPD of (±)Ibu$_2$HK with preferred orientation on the hkl plan (200), with a March–Dollase parameter of 0.6 (**top**) and an experimental XRPD of (±)Ibu$_2$HK and (±)IbuK (**bottom**). The strong first peak at 2θ = 4.13° corresponds to the (200) family of planes; the second highest at 2θ = 12.409° is the (600) family of planes. The top powder pattern is that of the potassium salt (±)IbuK previously obtained by Xu et al. To improve the visibility of low-intensity peaks, the most intense peaks have been truncated (//).

3.3. Hygroscopicity, Thermal Behaviors and Dissolution Behaviors of (±)IbuK and (±)Ibu$_2$HK

3.3.1. Stability vs. Relative Humidity

The behaviors of (±)IbuK and (±)Ibu$_2$HK as a function of RH were investigated by dynamic vapor sorption (DVS) at 25 °C (Figure 8). Each sample was first equilibrated at 0% RH to ensure complete dehydration, then subjected to one cycle of sorption–desorption between 0 and 90% RH (selected images of the (±)IbuK sample recorded during analysis are given in Figure S6).

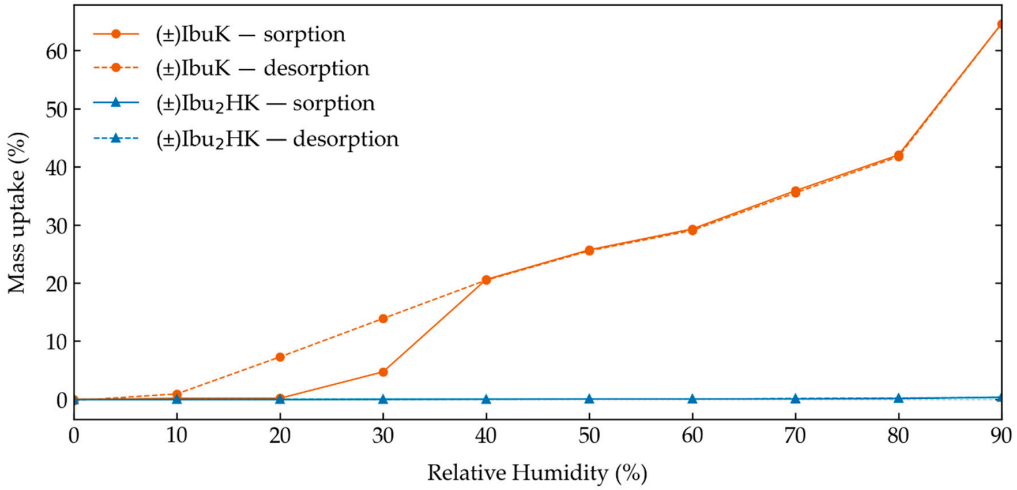


Figure 8. Comparative moisture sorption analysis of (±)IbuK (circles) and (±)Ibu$_2$HK (triangles) by DVS.

During sorption, the measurement on (±)IbuK has no noticeable mass gain up to 20% RH. At 40% RH and above, the mass uptake is continuous and substantial (up to 65% at 90% RH). This mass evolution associated with the macroscopic change of the powder indicates a deliquescent behavior of (±)IbuK (see Supplementary Materials-Figure S6). Despite conditioning at high RH, no hydrated form could be isolated. The desorption data follow the sorption curve, except for a small hysteresis between 10 and 40% RH, indicating the reversibility of the water uptake without formation of a hydrated phase.

This behavior classifies (±)IbuK as a highly hygroscopic salt with a critical relative humidity of deliquescence close to 40% at 25 °C.

By contrast, (±)Ibu$_2$HK shows neither hygroscopicity nor deliquescence over the investigated RH range (0–90% RH; Figure 8, triangles). At 80% RH, the reference condition used by the European Pharmacopoeia [28] to classify the hygroscopicity of solid APIs, the water uptake of (±)Ibu$_2$HK reaches only 0.19 wt%, against 42 wt% for (±)IbuK under the same conditions. On this scale, (±)IbuK is classified as very hygroscopic and deliquescent, whereas (±)Ibu$_2$HK is classified as non-hygroscopic.

3.3.2. Behaviors in Water

The evolution of (±)Ibu$_2$HK suspended in milli-Q water at 25 °C was monitored as a function of time. The evolution of the concentration and pH are given in the Supplementary Materials.

XRPD analysis of the solid sampled from the suspension revealed a solid-state transition occurring within the first minute of stirring of (±)Ibu$_2$HK in water (Figure 9). The most intense and characteristic Bragg peak (200) of (±)Ibu$_2$HK at 2θ = 4.13° decreased in intensity, while a new peak at 2θ = 6.10°, assigned to crystalline (±)IbuH, simultaneously emerged. Between 7 and 10 min, a steady state was reached in which the (200) peak of (±)Ibu$_2$HK was still observed with a low intensity while the rest of the diffraction pattern corresponded to (±)IbuH and remained unchanged for up to 72 h.

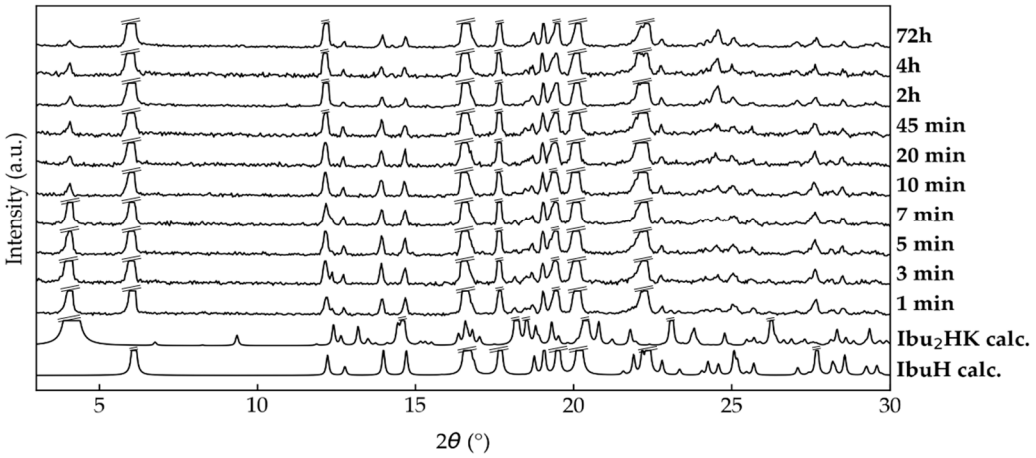


Figure 9. Solid-state evolution of (±)Ibu_2HK in aqueous suspension monitored by XRPD in the range of 1 min to 72 h with (±)IbuH and (±)Ibu_2HK (calculated) on the bottom as references. The most intense peaks corresponding to the family of planes (200) of (±)Ibu_2HK persist up to 72 h, while the rest of the pattern corresponds to (±)IbuH. To optimize the visibility of low-intensity peaks, the most intense peaks have been truncated (//).

The pH and the (±)IbuH concentration evolved in concert with this structural transformation, reaching a steady state within the first 30 min (Figure S7, Supplementary Materials).

(±)Ibu_2HK exhibits a full dissociation in water at 25 °C. In other words, (±)Ibu_2HK does not dissolve as a single entity but undergoes a solid-state transition into (±)IbuH. The highly soluble ionic species (±)Ibu^- and K^+ are released into solution within the first minute, while (±)IbuH, whose aqueous solubility is typically low, remains as a solid phase (Equation (1)).

$$(\pm)Ibu_2HK_{(s)} \rightarrow 0.5(+)(Ibu^-)_{solvated} + 0.5(-)(Ibu^-)_{solvated} + (K^+)_{solvated} + (\pm)IbuH_{(s)} \quad (1)$$

The subsequent slow dissolution of the remaining solid (±)IbuH then drives the system toward thermodynamic equilibrium, which is reached in less than 1 h and remains stable for at least 72 h. This dissolution profile can be described as a two-step dissolution, in which the rapid release of the ionic components within the first minute is followed by a slow, solubility-controlled release of (±)IbuH.

Dissolution experiments were repeated with different initial masses of (±)Ibu_2HK (from 1 to 70 mg) in 1 mL of milli-Q water at 25 °C. The steady-state pH and total solvated (±)Ibuprofen concentration after 72 h were determined by pH measurement and HPLC, respectively (available in Supplementary Materials). The observed variations in both pH and concentration as a function of initial mass are consistent with the full dissociation described above (Equation (1)). For concentrations higher than 1 $mg \cdot mL^{-1}$, the pH of the solution is always higher than the pKa because part of the (±)IbuH remains undissolved.

3.3.3. Thermal Behaviors and Stability

The thermal behaviors of (±)IbuK, (±)Ibu_2HK and (±)IbuH are compared in Figure 10. (±)IbuH displays a single sharp endotherm with an onset at 75.2 °C ($-104\ J \cdot g^{-1}$), in agreement with the value reported in the literature [29]. (±)IbuK exhibits a single endothermic event with onset at 227.5 °C ($63.7\ J \cdot g^{-1}$), also in agreement with a previous report on this compound ($T_{(\pm)IbuK}$ = 224–228 °C) [22].

Hot-stage microscopy (HSM) and TGA-DSC measurements were performed to clarify the nature of the high-temperature event observed for (±)Ibu_2HK (Figures 11 and 12). Upon heating beyond the melting point of (±)Ibu_2HK, two simultaneous phenomena were

observed in the (±)Ibu_2HK melt: (i) the evaporation of (±)IbuH, which condensed on the microscope lens and was identified by XRPD as recrystallized (±)IbuH, and (ii) the progressive recrystallization of (±)IbuK within the molten phase, also identified by XRPD on the recovered solid. The overall process can be summarized by Equation (2), which corresponds to a disproportionation:

$$(\pm)Ibu_2HK_{(l)} \rightarrow (\pm)IbuK_{(s)} + (\pm)IbuH_{(g)} \quad (2)$$

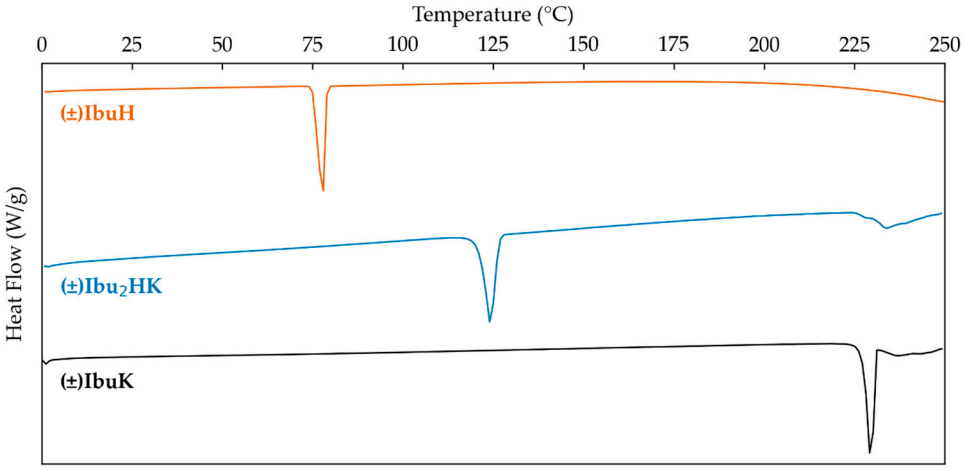


Figure 10. DSC thermograms of (±)IbuH (**top**), (±)Ibu_2HK (**middle**), and (±)IbuK (**bottom**) measured from 0 to 250 °C at a 2 K·min^{-1} heating rate.

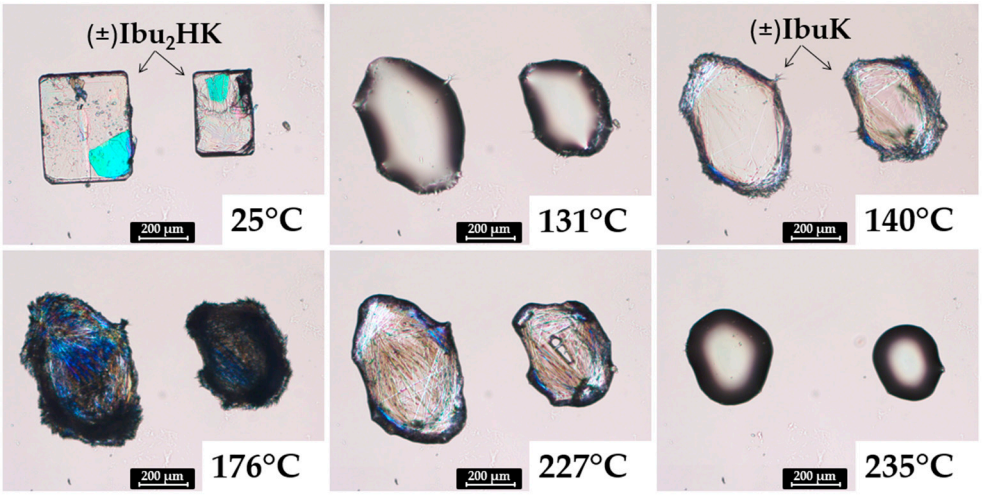


Figure 11. Hot-stage microscopy of (±)Ibu_2HK from 25 to 250 °C at 2K·min^{-1}. Illustrations of the sequential thermal events: melting of (±)Ibu_2HK, followed by the evaporation of (±)IbuH from melt (visible condensation), recrystallization of (±)IbuK, and final melting of (±)IbuK at a higher temperature.

TGA-DSC analysis supports this interpretation (from 20 °C to 250 °C at 2 K·min^{-1}, followed by a 2 h isotherm at 250 °C): a continuous mass loss of approximately 48.4% was recorded after melting, during the 2 h isothermal hold at 250 °C (the temperature was limited to 250 °C to prevent degradation), in good agreement with the theoretical fraction of one (±)IbuH within the (±)Ibu_2HK formula unit (45.8 wt%). Identical thermal behavior was observed for single crystals and powder samples (Figure S9). This thermally driven dissociation is consistent with the behavior in aqueous solution. Counterintuitively,

(±)IbuK has a high melting point while being highly soluble in water, whereas (±)IbuH has a low melting point and a poor aqueous solubility.

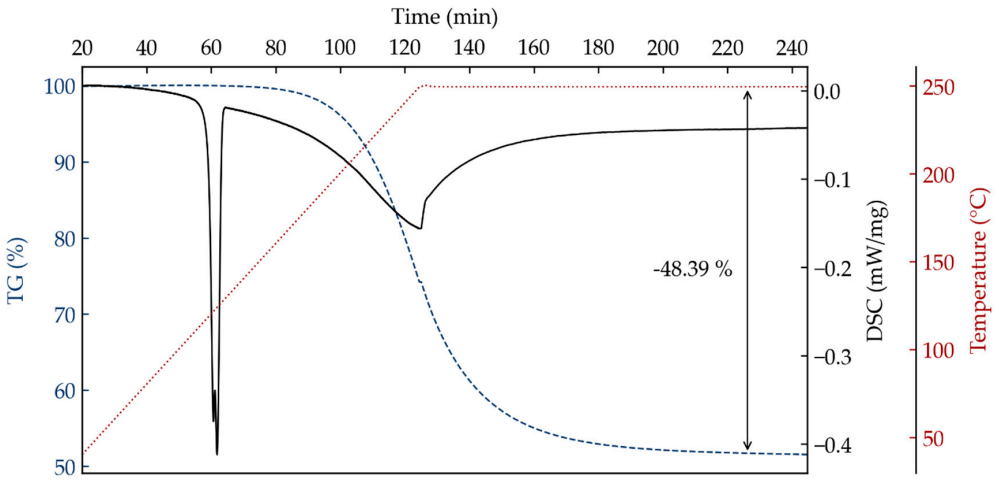


Figure 12. TGA-DSC vs. time analysis of (±)Ibu_2HK from 20 to 250 °C at 2 K·min^{-1}, followed by a 2 h isotherm at 250 °C. The blue dashed line represent the TG signal in % and the red dashed line represent the temperature in °C.

4. Conclusions

In this work, we report the synthesis, structural characterization and physicochemical behavior of (±)Ibu_2HK, a 2:1 hemi-salt of racemic ibuprofen with potassium. Single-crystal X-ray diffraction identifies (±)Ibu_2HK as a Speakman-type salt, with two distinct short O–H···O hydrogen bonds (O···O distances of 2.437 and 2.447 Å) connecting (±)IbuH and (±)Ibu^- units within the asymmetric unit. (±)Ibu_2HK also presents physicochemical characteristics markedly different from those of the equimolar salt (±)IbuK. Dynamic vapor sorption demonstrates that (±)Ibu_2HK is non-hygroscopic across the full 0–90% RH range, in contrast to the deliquescent behavior of (±)IbuK above 40% RH. Thermal analysis shows that the cocrystal salt melts congruently at 121 °C and then dissociates from the melt into (±)IbuK and volatile (±)IbuH, a behavior that highlights the hybrid character of this compound. In water, (±)Ibu_2HK fully dissociates into $0.5(+)(Ibu^-)_{solv}$ + $0.5(-)(Ibu^-)_{solv}$ + $(K^+)_{solv}$ and (±)IbuH, which precipitates. If the quantity of solvent is sufficient, it slowly redissolves, resulting in a two-step dissolution profile. To date, no potassium nor sodium cocrystal salt has been obtained from the pure enantiomers of ibuprofen. Taken together, these results illustrate the research pathway involved during solid-form screening. The ability of an API to form a given multicomponent phase, and the solid-state properties that result from it, cannot yet be reliably anticipated: they have to be assessed experimentally, form by form. In the present case, the 2:1 stoichiometry suppresses the deliquescence of (±)IbuK, but the aqueous behavior of (±)Ibu_2HK is governed by its full and fast dissociation. Based on the properties studied here—specifically, thermal behavior and behavior in aqueous media—the (±)Ibu_2HK compound offers only limited improvement compared to the (±)IbuK + (±)IbuH physical mixture, except for moisture sorption. While common in screening campaigns, this result remains valuable. Identifying a fully characterized new crystalline phase expands knowledge of the solid-state landscape of (±)ibuprofen, regardless of its development potential. Beyond the solid's intrinsic properties, various strategies—such as formulation—can be employed to provide additional leverage, supported by complementary fundamental analyses. More broadly, unconventional salt forms, such as hemi-salts and salt cocrystals, remain underutilized. Incorporating them into screening campaigns could broaden the range of accessible solid forms for ionizable active pharmaceutical ingredients beyond what conventional salt screening methods do.

Supplementary Materials: The following supporting information can be downloaded at: https://www.mdpi.com/article/10.3390/cryst16100607/s1, Figure S1: Overlay of the three independent molecules (same enantiomer), superimposed on their phenyl groups (Mol-O in gray, Mol-A in lime and Mol-B in purple). Hydrogen atoms are omitted for clarity. The To-1 and To-2 arrows indicate the torsion angles listed in Table S1. Table S1: Torsion angles measured on Mol-O, Mol-A and Mol-B for the same enantiomer: To-1 corresponds to O1-C1-C2-C4 and To-2 to C6-C7-C10-C11. Figure S2: Distribution of the equivalent isotropic displacement parameters (Ueq, $Å^2$) along the molecular skeleton of the three ibuprofen molecules in the asymmetric unit of (±)Ibu_2HK. Figure S3: Residual electron density in the difference Fourier maps around the two Speakman-type hydrogen bonds in (±)Ibu_2HK, after placement of the bridging protons at their geometrically calculated positions. (Left) Asymmetric type B pair (Mol-O···Mol-B), showing a single residual density maximum near the midpoint of the O···O vector. (Right) Symmetric type A pair (Mol-A···Mol-A′ across the inversion center at (½, ½, ½)), showing residual density distributed on both sides of the inversion center. Higher residual electron density values are shown in red and lower values in black/dark blue. Figure S4: Infrared (ATR-FTIR) spectra of (±)IbuH (top), (±)IbuK (middle) and (±)Ibu_2HK (bottom), recorded at room temperature in the 4000–400 cm^{-1} range with a resolution of 2 cm^{-1}. Reference [30]. Figure S5: (left) Projection of a single (*bc*) layer of (±)Ibu_2HK, built from potassium cations (K1 in blue, K2 in green) intercalated between ibuprofen dimers. The layer illustrates the extended two-dimensional connectivity between cations and carboxyl groups. (right) Dimers (circled in red) are connected along *b* and *c* axes by means of the potassium cations K1 (blue) and K2 (green). Figure S6: *In situ* optical images of (±)IbuK recorded during DVS analysis at 25 °C, showing the solid-state evolution as a function of relative humidity. Left (sorption): onset of deliquescence between ca. 30 and 40% RH, with progressive dissolution of the solid into a saturated aqueous solution. Right (desorption): progressive homogenization of the solution (30–20% RH), followed by recrystallization of (±)IbuK (20–10% RH). Figure S7: Time evolution during the dissolution of (±)Ibu_2HK in milli-Q water at 25 °C. (top) Supernatant pH; (bottom) solvated (±)ibuprofen concentration in the supernatant measured by HPLC. Figure S8: Steady-state pH (circles) and (±)IbuH concentration in the supernatant (squares) measured after 72 h of dissolution as a function of the initial mass of (±)Ibu_2HK (1 to 70 mg) added to 1 mL of milli-Q water at 25 °C. The dependence of both parameters on the initial mass reflects the coupled solubility equilibria described in the main text (Equation (1)). For concentrations higher than 1 $mg{\cdot}ml^{-1}$, the pH of the solution is always higher than the pKa because part of the (±)IbuH remains undissolved. Figure S9: Hot-Stage Microscopy of (±)Ibu_2HK powder from 25 to 250 °C at $2K{\cdot}min^{-1}$, illustrating the sequential thermal events occurring: melting of (±)Ibu_2HK followed by the evaporation of (±)IbuH from the melt (visible condensation), recrystallization of (±)IbuK, and finally the melting of (±)IbuK at higher temperature.

Author Contributions: Conceptualization, R.T., C.R., G.C. and E.C.S.; methodology, G.C. and E.C.S.; software, E.C.S.; validation, E.C.S., Y.C., M.S. and G.C.; formal analysis, E.C.S.; investigations, E.C.S., Y.C. and M.S.; data curation, E.C.S.; writing—original draft preparation, E.C.S.; writing—review and editing, E.C.S., R.T., C.R. and G.C.; visualization, M.S.; supervision, R.T., C.R. and G.C.; project administration, G.C.; funding acquisition, R.T. and C.R. All authors have read and agreed to the published version of the manuscript.

Funding: This research was funded by Sanofi and by the Association Nationale de la Recherche et de la Technologie (ANRT) through a CIFRE fellowship (CIFRE N°2023/0603).

Data Availability Statement: CCDC 2579228 contains the supplementary crystallographic data for this paper. These data can be obtained free of charge via www.ccdc.cam.ac.uk/data_request/cif accessed on 24 September 2026. On request, raw data of this research are available at gerard.coquerel@univ-rouen.fr.

Acknowledgments: The authors thank Nicolas Couvrat for TGA-DSC data collection and interpretation and Maxime Cazes for performing the XRPD measurements under dry air. Sanofi is thanked for supporting the PhD thesis of E.C.S. This work was supported by Sanofi and by the Association

Nationale de la Recherche et de la Technologie (ANRT) through a CIFRE fellowship (CIFRE No. 2023/0603), which is gratefully acknowledged.

Conflicts of Interest: ECS, CR and RT are employees of Sanofi and may own stock options in the company. The authors declare no conflicts of interest.

Abbreviations

The following abbreviations are used in this manuscript:

A^-	Deprotonated acid (carboxylate)
ANRT	Association Nationale de la Recherche et de la Technologie
API	Active pharmaceutical ingredient
CCDC	Cambridge Crystallographic Data Centre
CIFRE	Convention Industrielle de Formation par la Recherche
DSC	Differential scanning calorimetry
DVS	Dynamic vapor sorption
GOF	Goodness of fit
HA	Protonated (neutral) acid
HPLC	High-performance liquid chromatography
HSM	Hot-stage microscopy
(±)IbuH	Racemic ibuprofen, protonated form
(±)Ibu^-	Ibuprofenate anion
(±)IbuK	Racemic potassium ibuprofenate (1:1 salt)
(±)Ibu_2HK	Racemic ibuprofen–potassium ibuprofenate (2:1 cocrystal salt)
(±)IbuNa	Racemic sodium ibuprofenate
M^+	Metal cation
MeOH	Methanol
Mol-O, Mol-A, Mol-B	The three crystallographically independent ibuprofen molecules
pK_a	Logarithmic acid dissociation constant
PVDF	Polyvinylidene fluoride
RH	Relative humidity
R_1, wR_2, R_{int}	Crystallographic reliability factors
SCXRD	Single-crystal X-ray diffraction
SEM	Scanning electron microscopy
TGA	Thermogravimetric analysis
TGA-DSC	Thermogravimetric and differential scanning calorimetric analysis
XRPD	X-ray powder diffraction
Z, Z'	Number of formula units per unit cell and per asymmetric unit

References

1. Brittain, H.G. (Ed.) *Polymorphism in Pharmaceutical Solids*; Marcel Dekker: New York, NY, USA, 1999.
2. Peterson, M.L.; Hickey, M.B.; Zaworotko, M.J.; Almarsson, Ö. Expanding the Scope of Crystal Form Evaluation in Pharmaceutical Science. *J. Pharm. Pharm. Sci.* **2006**, *9*, 317–326. [PubMed]
3. Stahl, P.H.; Wermuth, C.G. (Eds.) *Handbook of Pharmaceutical Salts: Properties, Selection, and Use*; Wiley-VCH: Weinheim, Germany, 2002.
4. Shan, N.; Zaworotko, M.J. Polymorphic Crystal Forms and Cocrystals in Drug Delivery (Crystal Engineering). In *Burger's Medicinal Chemistry and Drug Discovery*; Wiley: Hoboken, NJ, USA, 2021; pp. 1–32.
5. Nijhawan, M.; Jidige, B.; Aleti, R.; Gunnam, S.; Saxena, T. Development and characterization of voriconazole-oxalic acid dihydrate cocrystals for enhanced pharmaceutical performance. *Prospect. Pharm. Sci.* **2025**, *22*, 199–203. [CrossRef]
6. Serajuddin, A.T.M. Salt Formation to Improve Drug Solubility. *Adv. Drug Deliv. Rev.* **2007**, *59*, 603–616. [CrossRef] [PubMed]
7. Grothe, E.; Meekes, H.; Vlieg, E.; Ter Horst, J.H.; De Gelder, R. Solvates, Salts, and Cocrystals: A Proposal for a Feasible Classification System. *Cryst. Growth Des.* **2016**, *16*, 3237–3243. [CrossRef]
8. Petruševski, G.; Naumov, P.; Jovanovski, G.; Bogoeva-Gaceva, G.; Ng, S.W. Solid-State Forms of Sodium Valproate, Active Component of the Anticonvulsant Drug Epilim. *ChemMedChem* **2008**, *3*, 1377–1386. [CrossRef] [PubMed]

9. Butterhof, C.; Milius, W.; Breu, J. Cocrystallisation of Benzoic Acid with Sodium Benzoate: The Significance of Stoichiometry. *CrystEngComm* **2012**, *14*, 3945–3950. [CrossRef]
10. Hu, M.; Lian, B. Synthesis, Structure and Characterization of a New Glycolate: Sodium Glycolate–Glycolic Acid (1/1). *Acta Crystallogr. C Struct. Chem.* **2026**, *82*, 60–67. [CrossRef] [PubMed]
11. Speakman, J.C. The Crystal Structures of the Acid Salts of Some Monobasic Acids. Part I. Potassium Hydrogen Bisphenylacetate. *J. Chem. Soc.* **1949**, *152*, 3357–3365. [CrossRef]
12. Speakman, J.C. Acid Salts of Carboxylic Acids, Crystals with Some "Very Short" Hydrogen Bonds. In *Structure and Bonding*; Springer: Berlin/Heidelberg, Germany, 1972; Volume 12, pp. 141–199.
13. Adams, S.S. The Propionic Acids: A Personal Perspective. *J. Clin. Pharmacol.* **1992**, *32*, 317–323. [CrossRef] [PubMed]
14. Hutt, A.J.; Caldwell, J. The Metabolic Chiral Inversion of 2-Arylpropionic Acids—A Novel Route with Pharmacological Consequences. *J. Pharm. Pharmacol.* **1983**, *35*, 693–704. [CrossRef] [PubMed]
15. Garzón, L.C.; Martínez, F. Temperature Dependence of Solubility for Ibuprofen in Some Organic and Aqueous Solvents. *J. Solut. Chem.* **2004**, *33*, 1379–1395. [CrossRef]
16. Avdeef, A. *Absorption and Drug Development: Solubility, Permeability, and Charge State*; Wiley-Interscience: Hoboken, NJ, USA, 2003.
17. Elder, D.P.; Holm, R.; Diego, H.L.D. Use of Pharmaceutical Salts and Cocrystals to Address the Issue of Poor Solubility. *Int. J. Pharm.* **2013**, *453*, 88–100. [CrossRef] [PubMed]
18. Lee, T.; Wang, Y.W. Initial Salt Screening Procedures for Manufacturing Ibuprofen. *Drug Dev. Ind. Pharm.* **2009**, *35*, 555–567. [CrossRef] [PubMed]
19. Shah, S.R.; Shah, Z.; Khan, A.; Ahmed, A.; Khwaja, S.; Csuk, R.; Anwar, M.U.; Al-Harrasi, A. Alkali complexes of non-steroidal anti-inflammatory drugs inhibit lung and oral cancers in vitro. *New J. Chem.* **2021**, *45*, 45–52. [CrossRef]
20. Censi, R.; Martena, V.; Hoti, E.; Malaj, L.; Di Martino, P. Sodium Ibuprofen Dihydrate and Anhydrous: Study of the Dehydration and Hydration Mechanisms. *J. Therm. Anal. Calorim.* **2013**, *111*, 2009–2018. [CrossRef]
21. Rossi, P.; Macedi, E.; Paoli, P.; Bernazzani, L.; Carignani, E.; Borsacchi, S.; Geppi, M. Solid–Solid Transition between Hydrated Racemic Compound and Anhydrous Conglomerate in Na-Ibuprofen: A Combined X-Ray Diffraction, Solid-State NMR, Calorimetric, and Computational Study. *Cryst. Growth Des.* **2014**, *14*, 2441–2452. [CrossRef]
22. Xu, X.; Erkoboni, D.F.; Lebo, D.B. Improved Forms of Pharmaceutically Active Agents and Method for Manufacture Thereof. Canadian Patent CA2410469A1, 3 October 2002.
23. Iafisco, M.; Morales, J.G.; Hernández-Hernández, M.A.; García-Ruiz, J.M.; Roveri, N. Biomimetic Carbonate–Hydroxyapatite Nanocrystals Prepared by Vapor Diffusion. *Adv. Eng. Mater.* **2010**, *12*, B218–B223. [CrossRef]
24. Bruker AXS Inc. *APEX4*, Version 2022.10-1; Bruker AXS Inc.: Madison, WI, USA, 2021.
25. Bruker AXS Inc. *SAINT*, Version 8.40B; Bruker AXS Inc.: Madison, WI, USA, 2021.
26. Farrugia, L.J. WinGX Version 2026.1 and ORTEP for Windows: An Update. *J. Appl. Crystallogr.* **2012**, *45*, 849–854. [CrossRef]
27. Sheldrick, G.M. A Short History of SHELX. *Acta Crystallogr. A* **2008**, *64*, 112–122. [CrossRef] [PubMed]
28. Council of Europe. Chapter 5.11: Characters Section in Monographs. In *European Pharmacopoeia (Ph. Eur.)*, 12th ed.; European Directorate for the Quality of Medicines & HealthCare (EDQM): Strasbourg, France, 2025.
29. Yuan, X.; Capomacchia, A.C. Influence of Physicochemical Properties on the In Vitro Skin Permeation of the Enantiomers, Racemate, and Eutectics of Ibuprofen for Enhanced Transdermal Drug Delivery. *J. Pharm. Sci.* **2013**, *102*, 1957–1969. [CrossRef] [PubMed]
30. Hadži, D.; Orel, B. The "OH Stretching" Band of Acid Salts of Carboxylic Acids and the Symmetry of the Hydrogen Bond. *J. Mol. Struct.* **1973**, *18*, 227–239. [CrossRef]

Disclaimer/Publisher's Note: The statements, opinions and data contained in all publications are solely those of the individual author(s) and contributor(s) and not of MDPI and/or the editor(s). MDPI and/or the editor(s) disclaim responsibility for any injury to people or property resulting from any ideas, methods, instructions or products referred to in the content.